Advances in Water Resources 187 (2024) 104693

Contents lists available at ScienceDirect

Advances in Water Resources

journal homepage: www.elsevier.com/locate/advwatres

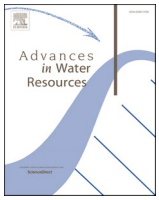

Revealing nitrate uptake and dispersion dynamics using high-frequency sensors and two-dimensional modeling in a large river system

Amirreza Zarnaghsh [a], Michelle Kelly [b], Amy Burgin [c], Admin Husic [a,*]

[a] Department of Civil, Environmental and Architectural Engineering, University of Kansas
[b] Department of Biological Sciences, Michigan Technological University
[c] Department Ecology and Evolutionary Biology and Kansas Biological Survey-Center for Ecological Research, University of Kansas

ARTICLE INFO

Keywords:
nitrate
aquatic sensors
numerical modeling
dispersion
diel cycling
water quality

ABSTRACT

Nitrate pollution of water bodies is a critical issue in many parts of the world because of its negative effects on aquatic ecosystem and human health. Effective management of pollution, such as the continuous or instantaneous release from point-sources, requires an understanding – with high spatial and temporal resolution – of how nitrate is dispersed and cycled within rivers. Nitrate sensing data show promise for this purpose, but their integration into numerical models is scarce; thus, questions remain regarding the necessary spatial grid size and temporal resolution required to resolve sensor readings. In this study, we developed an unsteady two-dimensional model to simulate nitrate transport, dispersal, and cycling along a 33-km stretch of the Kansas River (USA), following a strategic release of nitrogen from a decommissioned fertilizer plant. To validate modeled estimates of dispersion and uptake, we integrated 15-minute nitrate and temperature data from two aquatic sensors, one located proximal to the fertilizer release point and a second further downstream after complete lateral mixing. Model results at the site near to the contamination (0.4 km) were highly sensitive to river grid size and turbulent mixing, but insensitive to uptake. Results at the site far downstream of the contamination (31 km) were unaffected by grid size or mixing parameterization but were very sensitive to selection of uptake rate. High-frequency sensors allowed us to resolve diel variability in nitrate signals, which we incorporated into the model to improve performance and model realism. The 33-km study reach assimilated 14% of the total nitrate load in the river, or approximately half of what was contributed by the fertilizer release, during the two-month study period. Regarding nitrate cycling, modeled C_{diel}/C_{max} ranged from 0.04 to 0.11 whereas sensor observations showed much higher C_{diel}/C_{max} values of 0.11 to 0.25. Disagreements between data observations and model simulations in cycling are hypothesized to exist due to potential breakdown of the first-order rate kinetics. Together, our study shows the potential of combining numerical models and high-frequency data for a better understanding of the physical and biogeochemical processes that control nitrate dynamics in aquatic environments.

1. Introduction

Nitrate pollution in aquatic ecosystems is a significant environmental concern as it can lead to eutrophication, a process that results in the overgrowth of algae and other aquatic plants. This, in turn, can negatively impact water quality and cause oxygen depletion (Burns et al., 2019; Hansen and Singh, 2018; Kunz et al., 2017). One important mechanism of nitrate pollution in water bodies is the transport from a specific, identifiable source such as outfalls of wastewater treatment and industrial effluents, which is known as point-source pollution (Lee and Seo, 2010; Pilechi et al., 2016). Although this type of pollution has been extensively studied, the development of effective mitigation strategies is still limited by the challenge of predicting how nitrate is dispersed and cycled downstream (Huang et al., 2022; Velísková et al., 2014).

The physical transport and biogeochemical fate of nitrate in rivers is most often modeled using the Advection-Dispersion-Reaction Equation (Jan et al., 2021). While analytical methods have been developed to solve simplified cases of this equation (van Genuchten et al., 2013), numerical models are increasingly favored for more complex scenarios, particularly given the advances in computer technology (Ramezani et al., 2019; Velísková et al., 2014). One major challenge in using these models is the significant uncertainty associated with dispersion

* Corresponding author: Admin Husic, 2134B Learned Hall, University of Kansas, Lawrence, KS, 66045
E-mail address: ahusic@ku.edu (A. Husic).

https://doi.org/10.1016/j.advwatres.2024.104693
Received 25 October 2023; Received in revised form 26 January 2024; Accepted 5 April 2024
Available online 6 April 2024

coefficients and reaction rates, which are highly site-specific and subject to large spatial and temporal variability (Camacho Suarez et al., 2019; Shin et al., 2020). These parameters are typically determined through experimental methods (Baek and Seo, 2016; Knapp et al., 2017), empirical or theoretical relationships (Jeon et al., 2007), or model calibration to field-observed data (Gualtieri et al., 2017). For example, estimating turbulent fluxes requires definition of the turbulent Schmidt number (S_t, ratio of momentum diffusivity to mass diffusivity), but no universally accepted values exist and methodologies for its determination are still a topic of development (Gualtieri et al., 2017). While numerical models have contributed significantly to our understanding of nitrate transport in rivers, the temporal resolution of nitrate measurements used for calibration, i.e., daily to weekly, is often insufficient to capture the time scales of physical and biogeochemical processes that affect nitrate dynamics at sub-daily scales. This is particularly crucial in the mixing zone close to the pollutant source, where nitrate concentrations exhibit high variability in both space and time (Kim et al., 2011; Pilechi et al., 2016).

In-situ high-frequency sensors that measure water quality parameters every few minutes have opened new horizons in our understanding of aquatic hydrological and biogeochemical processes (Burns et al., 2019; Rode et al., 2016b; Zarnaghsh and Husic, 2023). Researchers have utilized high-frequency nitrate data to assess the primary sources and pathways of nitrate and analyze the impact of climatic and anthropogenic factors on in-stream nitrate dynamics (Dupas et al., 2016; Husic et al., 2023; Lloyd et al., 2016). Further, the widespread deployment of high-frequency nitrate sensors has yielded extensive insights into the diel variation in nitrate concentrations, which can be an indicator of nitrogen transformation processes including assimilation and denitrification (Kelly et al., 2021; Ledford and Toran, 2020). For example, sensor readings can resolve swings in nitrate that reflect assimilation by autotrophs during daylight hours and cessation during dark hours (Burns et al., 2019; Heffernan and Cohen, 2010) as well as heterotrophic uptake and release (Zhang et al., 2023). Despite the advantages of high-frequency nitrate data, they have not yet been integrated into models that predict the spread and cycling of point-source nitrate pollution. Given the increasing availability of high-frequency nitrate sensors and the large temporal variability of processes that affect the downstream transport of nitrate from local sources, it is both practical and logical to incorporate high-temporal resolution data into our models (Huang et al., 2022; Yang et al., 2023).

In this study, we incorporate high-frequency nitrate sensor data into the evaluation of a hydrodynamic model to gain insights into nitrate dynamics at fine temporal and spatial scales. Specifically, the objectives of this study were to model and sense how a controlled release of nitrogen from a decommissioned fertilizer plant disperses downstream and is taken up by aquatic biota in the Kansas River, USA. Over the course of three months, we collected 15-minute nitrate data from two locations downstream of the fertilizer release. We constructed a two-dimensional numerical model of water and nitrate transport along the Kansas River and calibrated it to the high-frequency sensing data at the two locations. We advance understanding of the dispersion and cycling of nitrate in large-river systems and provide recommendations for integrating sensor data into numerical model evaluation.

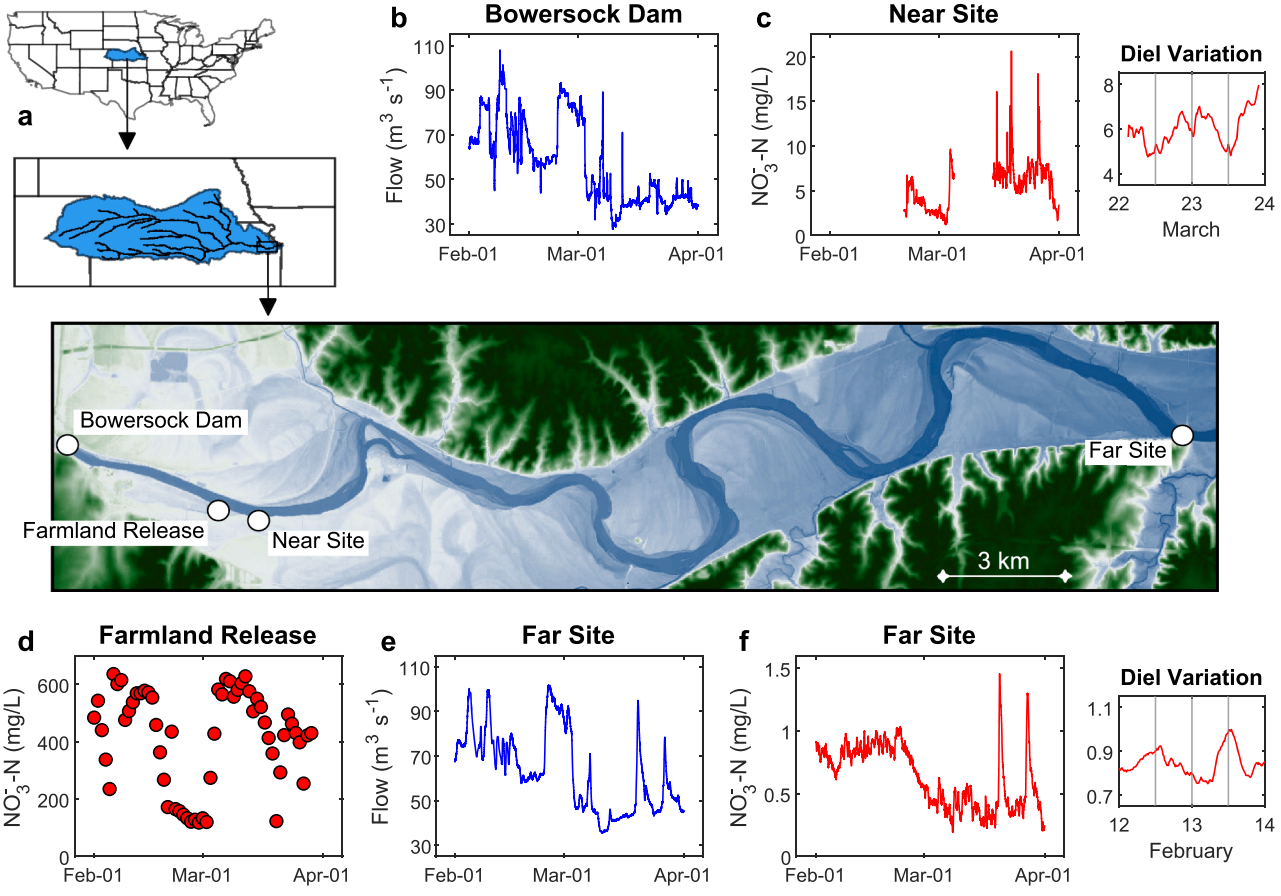

Fig. 1. (a) The Kansas River watershed is located in the central US, across the states of KS, CO, and NE. Our study corridor is situated between the cities of Lawrence (near "Bowersock Dam") and DeSoto, KS (near "Far Site"). Gaging stations, sensor locations, and Farmland Fertilizer Plant inputs are mapped. Time-series plots of discharge (b, e) and nitrate (c, d, f) are shown for the Bowersock Dam, Farmland Release, Near Site, and Far Site. Vertical bars in the diel variation subplots (c, f) indicate 12-hour increments, alternating between midnight and noon.

2. Study Site and Materials

2.1. Study Site

The Kansas River, located in northeastern Kansas, is a 274 km-long sand bed river that begins at the confluence of the Smokey Hill and Republican Rivers (Junction City, KS) and feeds into the Missouri River in Kansas City, MO (Fig. 1a). The river drains 155,000 km^2 of Kansas, Colorado, and Nebraska, has an average slope of less than 0.6 m per km, and is classified as an eighth-order, prairie, wide, and shallow river with an average width and depth of 164 m and 1.5 m, respectively. The mean annual flow recorded during the past twenty years in the Kansas River ranges from 55 m^3/s in 2003 to 640 m^3/s in 2019. The timing of flow in the Kansas River is regulated by releases from eighteen federal reservoirs that are located on major tributaries to the Kansas River, constituting approximately 80% of the basin's total drainage area. The reservoir releases are specifically crucial during a drought period like 2018 as they provide drinking water source for about 800,000 people in Kansas. The only major dam built on the mainstem of the Kansas River is the Bowersock Dam in Lawrence, KS, which hosts the only functional hydroelectric plant in the state and is located directly upstream of our study reach.

Starting in November 2017, and for a period of six months, the City of Lawrence, KS, was permitted to strategically release about 114 million liters of nitrogen-contaminated water from a decommissioned fertilizer plant (named "Farmland") into the Kansas River at a maximum rate of 1.9 million liters per day. The City's aim was to avert a potential uncontrolled overflow of fertilizer from the contaminated storage sites and into the Kansas River. The released water was heavily polluted with average nitrate and ammonia concentrations of 342 mg $NO_3^- - N\ L^{-1}$ and 125 mg $NH_4^+ - N\ L^{-1}$, respectively (Kelly et al., 2021). This planned discharge of highly contaminated waste served as a unique opportunity to conduct an experiment to understand the effects of point-source nitrogen pollution on physical dispersion and biogeochemistry in a large-river ecosystem. In this study, we analyze and model a 33.5 km reach of the Kansas River that was impacted by the release, extending from 2.5 km upstream of the release at Bowersock Dam to 31 km downstream of the release at DeSoto, KS.

2.2. Materials

Fifteen-minute discharge data were available at the upstream (USGS 06891080, Fig. 1b) and downstream (USGS 06892350, Fig. 1e) ends of our study region and provided the hydrologic boundary conditions for our water quality model. The high-frequency nitrate sensor data used for model evaluation in this study were collected and presented by Kelly and others (2021). Fifteen-minute nitrate data were collected from two locations, including one site that was monitored in Kelly et al. 2021 (starting three months after releases began, Fig. 1c) and one that is continuously operated by the USGS (Fig. 1f). The relative locations of the two sensors to the Farmland input include (1) a near-bank sensor 0.4 km downstream ("Near Site"), and (2) a mid-river sensor 31 km downstream at DeSoto ("Far Site"). Kelly and colleagues (2021) observed two additional locations as part of their research; however, these sites were excluded from this study due to factors such as effects near the dam, sensor burial, and malfunctions. These issues led to lower data quality and availability compared to the other sites.

The Near Site sensor was positioned on the proximal (right) bank of the river. It was hypothesized that this site would capture the highly dynamic physical dispersion of newly introduced nitrogen into the river, given its proximity to the release. The Far Site sensor was deployed from a bridge into the middle of the river, thus capturing prevailing flow conditions. It was hypothesized that because the Far Site is sufficiently downstream of complete river mixing, i.e., physical river mixing no longer dominates variations in nitrate concentration, it would capture greater information relative to biogeochemical uptake processes. The deployed nitrate sensors were fixed optical sensors with 2-mm path length and a detection limit of 0.1 mg-N L^{-1} (HACH Nitratax Plus SC, Loveland, CO, US). All quality assurance and controls steps taken for the high-frequency nitrate data are documented in Kelly and others (2021). The river width at the cross-sections where sensors were installed were 211 m and 138 m for the Near and Far Sites, respectively. Daily volume and nitrate concentrations (Fig. 1d) of farmland waste pumped into the river were obtained from the City of Lawrence.

3. Methods

The two-dimensional (2D) flow and nitrate domains in our study area were simulated using the MIKE 21 FM model, which was developed by the Danish Hydraulic Institute (DHI). MIKE 21 FM employs a Flexible Mesh (FM), cell-centered Finite Volume spatial discretization scheme with unstructured triangular grids throughout the model region. This approach was selected as it provides more geometric flexibility and the possibility of altering the resolution at certain areas of interest in the model. In this study, we utilized the hydrodynamic (HD) and transport (TR) modules in MIKE 21 FM to simulate the river flow and transport/cycling of nitrate, respectively. Further, we used lower order schemes for both spatial and time integration in our model due to availability of time and computational resources. More details on the MIKE 21 FM modelling can be obtained in the technical notes published by DHI (Danish Hydraulic Institute, 2019).

Overall, our research procedure can be summarized as follows: 1) the hydrodynamics model was developed, calibrated, and validated to observed river discharge, and 2) with confidence in the validity of the hydrodynamic processes, a transport model for dispersion and cycling of nitrate was constructed. Then, 3) a grid sensitivity analysis was performed to find the most appropriate grid resolution for the model to accurately capture nitrate sensor observations, and 4) physical nitrate dispersion was calibrated and the sensitivity of the model results to turbulent mixing was explored. Finally, 5) biochemical nitrate uptake was calibrated to the observed high-frequency diel nitrate fluctuations that occur due to temperature and light dependency of riverine biota.

3.1. Water Model

3.1.1. Numerical Model Equations

The MIKE 21 FM hydrodynamic module solves the depth-averaged Saint-Venant equations (1,2,3) to obtain the water depth and velocity components:

$$\partial_t h + \partial_x(hu) + \partial_y(hv) = S \tag{1}$$

$$\partial_t(hu) + \partial_y(huv) + \partial_x\left(hu^2 + \frac{gh^2}{2}\right) = gh\left(S_{0x} - S_{fx}\right) \tag{2}$$

$$\partial_t(hv) + \partial_x(huv) + \partial_y\left(hv^2 + \frac{gh^2}{2}\right) = gh\left(S_{0y} - S_{fy}\right) \tag{3}$$

where h is the water depth, (u, v) are the longitudinal and transverse depth-averaged velocities, g is the gravitational constant, S is the source term, S_{0x} and S_{0y} are the water surface gradients, $S_{fx}$and S_{fy} are the roughness terms (depending on the roughness law), and z is topography. These equations are the simplified version of the Navier-Stokes equations that are valid assuming: 1) negligible velocity components and hydrostatic pressure distribution in the vertical direction, 2) incompressible and homogenous fluid, and 3) small channel slopes. Our study satisfies these assumptions as the 33-km stretch of Kansas River we study is a shallow, wide river with a mean bed slope of 0.0004 m/m.

3.1.2. Data inputs, boundary conditions, and model uncertainty

Resolving the physics of water flow relies on high quality

topographic data. We combined aerial 2-m resolution digital elevation models (AIMS, 2020) with bathymetric cross-sectional surveys of the Kansas River (personal communication with USACE, 2022) to constrain topographical inputs. The numerical grid was developed using the mesh generator tool in MIKE 21 FM with an average grid resolution of 20-m and a total number of grid cells on the order of 15,000 (Figure S1). The boundary conditions for the model included the upstream discharge at the Bowersock Dam and the downstream free outflow at the DeSoto. The daily discharge of waste effluent into the river was added as a "varying in time" point-source discharge. Groundwater inputs were not considered due to a lack of available data for parameterization and a satisfactory closing of the water budget to within 5% for the 33-km reach using only the upstream river and waste inputs. The critical Courant-Friedrichs-Levy (CFL) number was set at 0.8 and a time step interval of 30 seconds was used for the simulations. Density was assumed to be barotropic (not a function of salinity and temperature) and a flux based Smagorinsky formulation was selected to represent the horizontal eddy viscosity with a default Smagorinsky constant value of 0.28 m^2/s. The riverbed resistance was represented by a constant Manning roughness value that was calibrated to optimize flow prediction. Model goodness of fit was based on comparison of modeled versus observed discharge using the Kling-Gupta Efficiency (KGE), which we define below in Section 3.2.3.

3.2. Nitrate Model

3.2.1. Numerical Model Equations

Using the hydrodynamic parameters of the river (h, u, v), we simulated the dispersal and fate of nitrate using the depth-integrated conservation equation for a scalar quantity:

$$\frac{\partial hC}{\partial t} + \frac{\partial huC}{\partial x} + \frac{\partial hvC}{\partial y} = hF_C - hk_pC + hC_sS \quad (4)$$

where C is the depth-averaged nitrate concentration, k_p is the nitrate decay/uptake rate, S is the load of nitrate source discharged by the fertilizer release, C_S is the nitrate concentration in the source, F_C is the horizontal dispersion term and calculated as $\left[\frac{\partial}{\partial x}\left(D_H\frac{\partial}{\partial x}\right) + \frac{\partial}{\partial y}\left(D_H\frac{\partial}{\partial y}\right)\right]C$, and D_H is the horizontal dispersion coefficient. Of particular interest for pollutant modeling, and one goal of this study, is the estimation of D_H and k_p.

Dispersion is parameterized with a scaled eddy viscosity approach as:

$$D_H = \nu_t/S_t \quad (5)$$

where ν_t is the sub-grid scale eddy viscosity and S_t is the turbulent Schmidt number. The eddy viscosity can be calculated using the Smagorinsky formulation as $C_s^2\Delta^2\sqrt{2S_{ij}S_{ij}}$, where C_s is Smagorinsky constant, Δ is the characteristic length of the grid, and S_{ij} is the deformation tensor (Rodi, 2000). The turbulent Schmidt number represents the ratio of momentum diffusion to mass diffusion and is analogous to the turbulent Prandtl number. An exact formulation for S_t is not well-established given its turbulent nature, thus it is often calibrated to data observations; typical S_t values for open channel flows range from 0.2 to 2.1 (Gualtieri et al., 2017).

Nitrate uptake is parameterized with a modified first-order kinetics formulation as:

$$k_p = k_{ref}f_{day}Q_{10}^{(T - T_{ref})/10} \quad (6)$$

where k_{ref} is the reference uptake rate for T = 15°C, f_{day} is a linear function bound from 0 (pre-dawn, lowest reactivity) to 1 (near-dusk, greatest reactivity) to simulate diel variations in uptake, Q_{10} is the temperature coefficient that describes the rate of reaction increase with every 10°C rise in temperature, T is the water temperature, and T_{ref} is the reference temperature. Q_{10} and T_{ref} for nitrate uptake were determined from the literature as 3.1 and 15°C, respectively (Reay et al., 1999). As k_p varies with temperature, we report a bulk uptake rate $\bar{k}_p$, which represents the mean uptake integrated over the study period. While removal can occur via pelagic and benthic algae as well as bacteria, MIKE-21 parameterizes a single rate for all reactions, thus this reflects the combined effects of multiple processes and interfaces. Later, we discuss how we vary these two parameters (S_t and $\bar{k}_p$) over a wide range derived from the literature to calibrate them and test their sensitivity. We constrain the uncertainty related to determining S_t and $\bar{k}_p$ using aquatic sensors positioned close to and far from the waste release, respectively.

3.2.2. Data inputs and boundary conditions

The upstream boundary condition for the model defines a 'background/ambient' nitrate concentration that exists in the river prior to contamination by the fertilizer addition at Farmland. Originally, we intended to use a nitrate sensor at Bowersock Dam as the upstream input, but due to sensor interference these data were rendered unusable (Kelly et al., 2021). Instead, daily grab sample data collected by the City of Lawrence from Burcham Park, approximately 0.5 km upstream of the Bowersock Dam, were used (Figure S2). These samples were collected from the bank of the river near a slow-moving portion of the flow, which may not fully represent nitrate concentrations across the river-width. Thus, we averaged data collected during high flow conditions, where local effects are expected to be minimized, and set this as a constant upstream input for the month of February (Figure S2). For March, during the low-flow period (3/5/2018 – 3/31/2018), all samples collected at Burcham Park were below the detection limit due to local bank effects. To overcome this, we adopted a constant background concentration for this period, equivalent to the lowest concentration measured by a high-frequency sensor located at the Far Site (Figure S2). The Farmland Release was treated as a point-source. While the Farmland Release was composed of both nitrate and ammonium, only nitrate was detected in the downstream river (most ammonium samples were below detection limit; Kelly et al., 2021). Thus, we assumed rapid nitrification of ammonium, and we combined the NH_4^+ and NO_3^- loads into a single point source of NO_3^-. Once the nitrate concentrations of the upstream inflow and point source were determined, the dispersion and uptake processes could then be modeled to simulate the evolution of the nitrate plume in the downstream direction. As part of the numerical scheme, as in the hydrodynamic model, we used a zero gradient (Neumann) boundary condition for the downstream section of the transport model.

3.2.3. Model calibration and uncertainty

Model performance was evaluated by comparing the simulated nitrate concentrations to the observed timeseries recorded by the sensors at the two sites. To achieve the best-performing numerical model, we considered and assessed the sensitivity of three components that exert control over simulated concentrations: the resolution of the numerical grid, the value of the turbulent Schmidt number (S_t), and the uptake/decay ($\bar{k}_p$) rate. First, in the immediate downstream vicinity of the Farmland Release, contaminated waste material on the order of 100s of mg-N/L rapidly mixes with background nitrate concentrations of less than 1 mg-N/L. To resolve the large mixing gradients that occur in this area, a finer resolution mesh is necessary than is required further downstream, where concentration gradients are much lower. Therefore, we determined the appropriate numerical grid resolution to resolve sensor readings using six different grid sizes ranging from 2.5 m to 20 m around the release point and the Near Site. Second, to evaluate the model's sensitivity to the selection of the horizontal dispersion coefficient (D_H), which depends on S_t, we assessed four different values of S_t (0.25, 0.50, 1.00, and 2.00), spanning the range reported in the literature (Gualtieri et al., 2017). Third, to fine-tune the modeled uptake of nitrate, we varied the decay rate ($\bar{k}_p$) between a value of zero (conservative transport) and several values near the upper bound of estimates

reported in the literature (0.12, 0.24, and 0.36 1/d). Once the uncertainty related to grid size, dispersion, and uptake was resolved, we used the optimal value for each of the three components to create a 'best run' for the model simulation. The non-optimal combinations of grid size, dispersion, and uptake were used to create uncertainty bounds for the 'best run' prediction. To test the influence of biochemical uptake to the overall nitrate concentration, we compared results from our optimized reactive transport model to those of a conservative model where $\overline{k}_p = 0$.

We compared the relative influence of transport time and reaction time at each site by calculating the Damköhler number (D_a) as

$$D_a = \tau_{trans}/\tau_{react} \quad (7)$$

where τ_{trans} represents the transport timescale ($\tau_{trans} = L_t/\overline{u}$) and τ_{react} represents the reaction timescale ($\tau_{react} = 1/\overline{k}_p$). L_t, $\overline{u}$, and $\overline{k}_p$ are representative length scales, mean streamwise velocities, and reaction rates, respectively, at the two sites. L_t is equal to 400 m for Near Site and 31,000 m for far site. $\overline{u}$ is equal to 0.12 m/s for the Near Site, which is close to a streambank, and 0.61 m/s for the Far Site, which is situated in the channel thalweg. $\overline{k}_p$ is equivalent for both sites and is to be determined through model calibration. A value of D_a equal to 1 bifurcates nitrate dynamics into transport ($D_a < 1$) or reaction ($D_a > 1$) dominated processes (Ocampo et al., 2006).

To quantify the goodness-of-fit of our modeled simulations, we evaluated performance using the Kling-Gupta efficiency (KGE), which is calculated as:

$$KGE = 1 - \sqrt{(r-1)^2 + (\alpha-1)^2 + (\beta-1)^2} \quad (8)$$

where r, α, and β are the correlation, standard deviation, and bias terms, respectively. r is calculated as $cov(x_s,x_o)/\sigma_s\sigma_o$, α is calculated as σ_s/σ_0, and β is calculated as μ_s/μ_0 (Gupta et al., 2009). The mean and standard deviation terms are represented by μ and σ, respectively, while "o" and "s" represent observations and simulations, respectively. To further assess model goodness-of-fit, we compare the modeled versus observed relative magnitudes of diel nitrate swings (C_{diel}/C_{max}) at the Far Site. Biochemical effects, which are mediated by temperature and light, cause distinct diel swings in riverine nitrate (C_{diel}), from a maximum concentration in the pre-dawn hours (C_{max}) to a minimum concentration in the near-dusk hours. Prior to calculating C_{diel}, a third-order, 12-hour Savitzky-Golay filter was used to smooth nitrate sensor readings and remove the influence of transient fluctuations in sensor readings while leaving intact dominant trends. A beta distribution, bound between 0 and 1, was used to plot the distribution of C_{diel}/C_{max} for comparison between data observations and model simulations. Lastly, due to relatively short period of our study (two months) and unique nitrate pollution conditions, we used the entire length of data for calibration without a separate validation dataset. Recent research has suggested that the traditional split-sample approach may not always be necessary (Shen et al., 2022), hence we proceed with the stated evaluation approach.

4. Results

4.1. Water Model

Hydrology in the Kansas River is heavily influenced by upstream reservoirs, which have dammed approximately 80% of the river's drainage basin and serve to store water during the wet season and release it during the dry season. Therefore, spikes in the hydrograph are associated with reservoir water releases as much as they are with runoff arrival (Fig. 1 b, c). Winter in the Kansas River basin is a period of less precipitation compared to summer, but because of reservoir releases, flows are higher during the late winter period (February, average flow of 75.6 m^3/s) than they are in the early spring (March, average flow of 46.2 m^3/s). Flow in the river was dynamic due to releases from upstream reservoirs (Figure S3) as well as four significant precipitation events ($P_{total} > 4cm$), which occurred on Feb. 2, Feb. 9, Mar. 19, and Mar 26. This unique hydrology influences the depth, velocity, and timing of water transport in our 33-km modeling domain.

The hydrodynamic model we developed does exceptionally well to simulate flow transport dynamics from Bowersock Dam to DeSoto during our two-month study period (KGE = 0.89; Fig. 2). Discharge peaks are well captured by the model for most parts of the high flow period, but with some underestimation during the latter months. The calibrated Manning's *n* was 0.045 although sensitivity analyses showed negligible dependence of the results on the selection of Manning's *n* (varied from 0.02 to 0.06). Flow depths were generally larger in the upstream portion of the study reach compared to the rest of the reach (Fig. 2). The mean depth-averaged velocities at the near-bank and mid-river sensor sites were 0.12 m/s and 0.61 m/s, respectively. Successful simulation of river hydraulics in our study section gave us confidence to carry forward these results into a simulation of nitrate biochemistry.

4.2. Nitrate Model

4.2.1. High-frequency data observations

Much like the hydrology of the Kansas River, reservoir releases impart considerable influence on the overall magnitude of nitrate concentration in the river (Fig. 1). The Far Site represents the net-effect of background nitrate delivered by reservoir releases and runoff as well as nitrate waste additions from Farmland. For this reason, three distinct periods in nitrate concentration occur at the Far Site: (1) elevated concentrations in February, (2) lower concentrations in March, and (3) nitrate spikes during two storm events in March (Fig. 1f). Nitrate concentrations in the river are greater when reservoir releases are high ($\overline{C} = 0.82$ mg-NL^{-1} and $\overline{Q}_{releases} = 56$ m^3/s in February) versus when they are low ($\overline{C} = 0.46$ mg-NL^{-1} and $\overline{Q}_{releases} = 22$ m^3/s in March), indicating the importance of reservoir releases to background riverine nitrate concentrations. In late March, several nitrate spikes in concentration likely represent the delivery of agricultural runoff from within the 33-km study section, as several large discharge events were observed in the downstream gage (Fig. 1e), but not at the upstream gage (Fig. 1b). At the Near Site, nitrate concentrations were an order of magnitude larger ($\overline{C} = 5.3$ mg $- N L^{-1}$) than at Far Site ($\overline{C} = 0.63$ mg $- N L^{-1}$) due to the proximity of the Near Site to the Farmland release (Fig. 1c). During February, when reservoir contributions are high, the nitrate concentrations at Near Site were relatively small ($\overline{C} = 3.58$ mg $- N L^{-1}$) due to dilution by large quantities of reservoir water. However, during the second half of the study period, when reservoir contributions decrease, the fertilizer waste constitutes a larger fraction of total river flow thus the Near Site had greater nitrate concentrations ($\overline{C} = 6.15$ mg $- N L^{-1}$).

Diel behavior varied both in terms of timing and magnitude at the two sites (Fig. 3). At the Near Site, the normalized diel (C/C_{max}) curve typically crested at around 6 AM with the trough following 8 hours later at 2 PM. This behavior is typical of uptake mediated by phototrophs. On the other hand, at the Far Site, the inverse was observed; the trough of the C/C_{max} curve occurred at around 6 AM with the crest occurring 8 hours later at 2 PM, suggesting other drivers. Regarding the magnitude of C_{diel}/C_{max}, the Near Site had relatively greater swings (median: 0.27) than did the Far Site (median: 0.13) over the two-month study period. The Near Site showed little variability in median C_{diel}/C_{max} from February (0.28) to March (0.26), whereas median C_{diel}/C_{max} at the Far Site varied more considerably from February (0.11) to March (0.23). It is important to note that the diel patterns in Fig. 3 are not from a single event, but rather represent the median C/C_{max} at a given timestep from all observed diel patterns at a site during the study. With an understanding of nitrate dynamics informed by high frequency sensor data, we proceed to model the dispersion and uptake of nitrate in the river corridor.

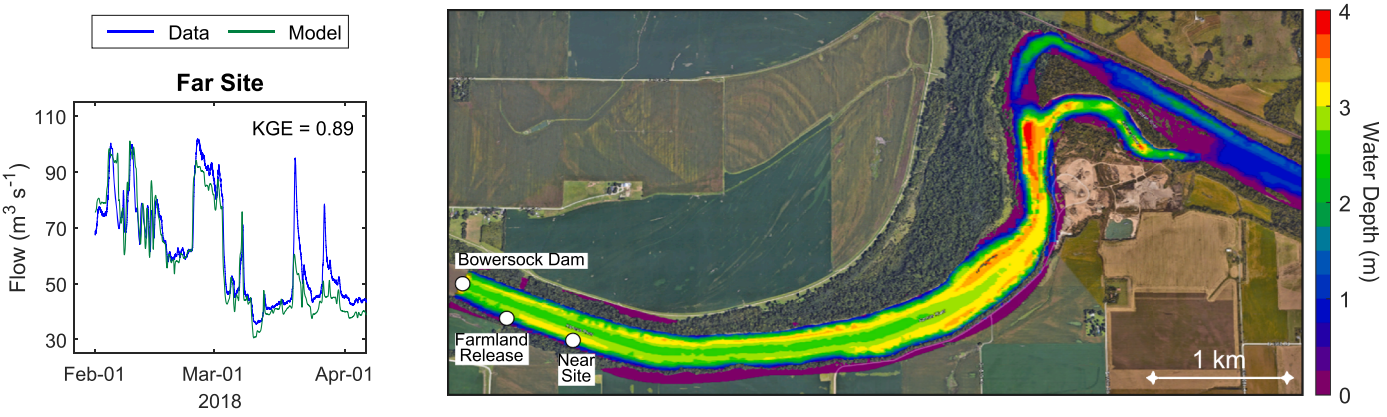

Fig. 2. Time-series of modeled versus observed discharge at the downstream Far Site (left panel). Modeled flow depths during a highly inundated period on February 8, 2018, which show a sequence of pools and riffles around a meander (right panel). KGE = Kling-Gupta Efficiency.

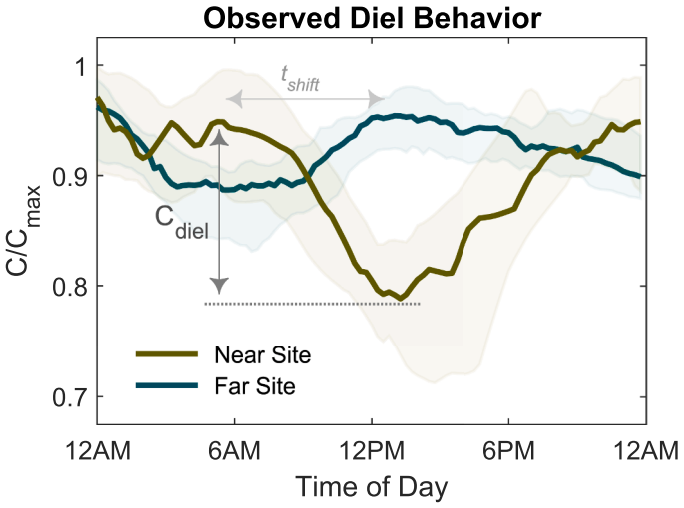

Fig. 3. Observed diel nitrate variation (C_{diel}), at the Near Site and Far Site, normalized to daily maximum concentration (C_{max}). Solid lines and shaded regions represent the median and 25th percentile bounds of C/C_{max}, respectively, calculated at each timestep for all days at a site. The eight-hour shift in the daily peak C between the sites is denoted by t_{shift}.

4.2.2. Numerical model simulations

The optimal nitrate model, which includes both physical and biochemical processes, has very good performance at the Near Site (KGE = 0.76) and the Far Site (KGE = 0.70) and captures the order-of-magnitude difference in nitrate concentrations between the sites and the temporal evolution of concentrations at each site (Fig. 4). Close to the Farmland Release (inset panel in Fig. 4), nitrate gradients are extremely high, with fertilizer effluent ($\overline{C} \approx 500$ mg N L^{-1}) rapidly mixing with the ambient river water ($\overline{C} = 0.46$ mg N L^{-1}). The volumetric discharge of fertilizer effluent is quite small ($\overline{Q} \approx 0.02$ m^3 s^{-1}) compared to the total river discharge ($\overline{Q} = 61.5$ m^3 s^{-1}), but because of the nearly 1000-fold difference in concentrations, the effluent dramatically alters the river's nitrate chemistry and raises overall river concentrations (from 0.46 to 0.63 mg N L^{-1}). The Near Site is located 0.3 km downstream of the Farmland Release, on the same side of the riverbank, and concentrations reduce substantially by this point (down from $>$ 500 to 5.4 mg N L^{-1}) as the fertilizer release is diluted and mixed. Near-complete lateral mixing is achieved around the first major bend in the Kansas River, approximately 4.5 km downstream of the release, after which biochemical uptake – rather than turbulent mixing – becomes prominent in controlling longitudinal and temporal variation in nitrate concentrations.

We simulated conservative transport conditions, i.e., dispersion occurs but not uptake ($k_p = 0$), to assess the importance of biological activity in the river. Model results for the conservative condition (KGE = 0.69) are nearly identical to the optimal model results (KGE = 0.70), which include uptake (Fig. 4). Despite similarity in the model performance metrics, the conservative model generally over-estimates concentrations, which the inclusion of uptake improves upon. Further, only the reactive model emulates the biologically driven diel fluctuations of nitrate that are observed in the data (Fig. 5). In February, the sensor data showed that median C_{diel}/C_{max} was 0.11 compared to 0.04, 0.06, and 0.08 for the low, medium, and high k_p values, respectively. In the warmer month of March, the sensor data showed that median C_{diel}/C_{max} was 0.23 compared to 0.07, 0.08, and 0.11 for the low, medium, and high k_p values, respectively. Slightly larger modeled estimates of C_{diel}/C_{max} occur in March compared to February, which are attributed to temperature-driven effects on first-order kinetics ($\Delta T = +6.2$°C in March). However, the observed C_{diel}/C_{max} values show a dramatic increase from 0.11 to 0.23, which cannot be attributed entirely to temperature changes. Regarding the timing of C/C_{max}, our model similarly showed a mid-day crest in the diel curve at around 1 PM (not plotted), similar to the data observed at Far Site (Fig. 3) but with a less pronounced C_{diel} magnitude, as discussed earlier.

4.2.3. Model evaluation and uncertainty

To obtain the best nitrate model estimates and assess the uncertainty in the selection of triangular grid resolutions, turbulent Schmidt numbers (S_t), and nitrate uptake rates ($\overline{k}_p$), we varied these model parameters over a specific range to conduct a sensitivity analysis (Tables 1 and 2). Our results indicated that model performance at the Near Site is quite sensitive to the selection of grid resolution and moderately sensitive to the selection of S_t (Table 1). On the other hand, the Near Site is not at all sensitive to $\overline{k}_p$ due the dominance of physical processes near the release (Table 2). Regarding the Far Site, model performance is sensitive to the selection of $\overline{k}_p$, but not to the selection of grid size or S_t due to the site being far downstream of where complete mixing has occurred. The Damköhler number (D_a) was an order of magnitude greater at the Far Site (0.210) compared to the Near Site (0.014), suggesting that the relative importance of reaction processes grows as material travels further downstream. Thus, the Near Site was used to fine-tune physical processes while the Far Site was used to fine-tune biochemical processes.

The grid sensitivity analysis was performed using six different grid sizes ranging from 2.5 m to 20 m. For the Near Site, we obtained the best model results with the 4.5 m grid, with the grid resolutions larger and smaller than this value leading to overestimation and underestimation of the nitrate concentrations, respectively. For example, the peak nitrate concentration occurred on Mar. 19 and was estimated as 0.75 mg/L

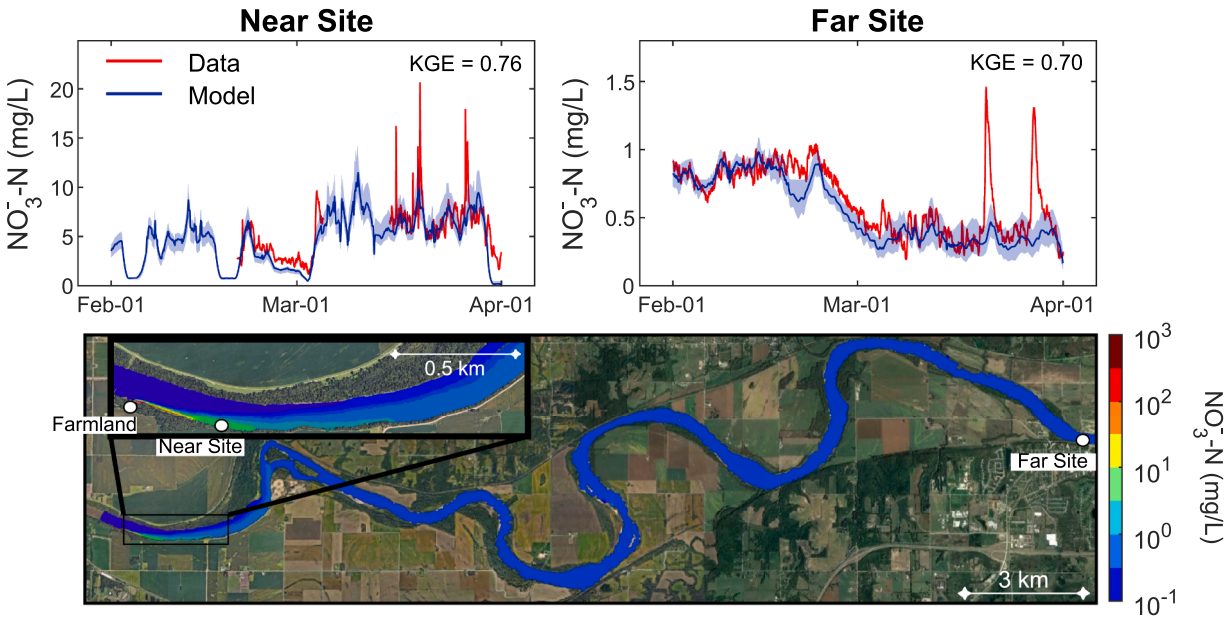

Fig. 4. Calibrated nitrate model results at the Near and Far Sites during the spring of 2018. Shading represents uncertainty bounds on model outputs. A spatial map of nitrate predictions is also shown for the wettest day of the study period February 25, 2018, with an inset to highlight large concentration gradients near the Farmland Release. KGE = Kling-Gupta Efficiency.

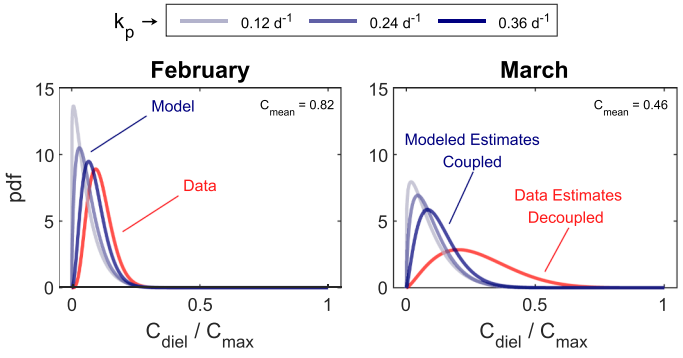

Fig. 5. Comparison of observed and modeled diel nitrate variation, C_{diel}, normalized to daily maximum concentration, C_{max}, at the Far Site. Model results are shown for three different uptake rates (k_p, 1/d). Modeled results of C_{diel}/C_{max} are similar between February and March with a slight increase in March due to warmer waters and increased rates. On the other hand, data results show a decoupling of C_{diel}/C_{max} between February and March, which cannot be attributed to temperature changes alone, indicating non-first order processes. The units of C_{mean} are mg-N/L.

Table 1
Sequential evaluation of model sensitivity to physical parameters: grid resolution and turbulent Schmidt number (S_t). Grid size was calibrated first. Thereafter, S_t was calibrated second. The optimal parameterization at each step in the sequential evaluation is indicated by **bold** font. KGE = Kling-Gupta Efficiency.

Grid Size (m)	Near Site (KGE)	Far Site (KGE)	S_t (-)	Near Site (KGE)	Far Site (KGE)
20	-0.35	0.72	for grid size = 4.5 m		
10	0.06	0.69			
5	0.60	0.73	0.25	0.42	0.68
4.5	**0.76**	**0.70**	0.5	0.68	0.69
3.8	0.65	0.71	**1**	**0.76**	**0.69**
2.5	-0.22	0.71	2	0.59	0.69

Table 2
Evaluation of model sensitivity to the biochemical parameter: mean uptake rate ($\bar{k}_p$). Physical process optimization of grid size and S_t is inherited from Table 1. The optimal parameterization for biochemical uptake is indicated by bold font. KGE = Kling-Gupta Efficiency.

$\bar{k}_p$ (d^{-1})	Near Site (KGE)	Far Site (KGE)
for grid size = 4.5 m and S_t = 1.00		
0	0.76	0.69
0.12	**0.76**	**0.70**
0.24	0.76	0.62
0.36	0.76	0.54

using a 20 m grid or 19.66 mg/L using a 2.5 m grid, indicating the significance of selecting a proper spatial discretization for the area close to the release point. For the Far Site, however, we got satisfactory results regardless of the choice of the grid resolution, as indicated by the KGE difference smaller than 0.04 between the best and worst results at this site (Table 1).

The nitrate dispersion sensitivity analysis was performed using four different S_t values (0.25, 0.50, 1.00, and 2.00; Table 1). The best model performance at the Near Site was obtained with an S_t of 1.00 for the Near Site (KGE = 0.76). In contrast, at the Far Site, we observed very small dependence of KGE on S_t across all simulations (maximum KGE difference of 0.01). The length required for full mixing of the released nitrate across the channel ranged from 3.6 km for 19.9 km, in models using 2.00 and 0.25 as the S_t values, respectively, indicating that by the time the nitrate plume arrives to the downstream location, it has been fully mixed for at least 10 km irrespective of parameterization.

By fixing the grid resolution and S_t values to 4.5 m and 1.00, respectively, we analyzed the impact of $\bar{k}_p$ on nitrate concentrations at the Far Site by varying $\bar{k}_p$ between 0 and 0.36 1/d. At conservative transport conditions ($\bar{k}_p = 0$) and at the lowest uptake rate ($\bar{k}_p = 0.12$ 1/d), model performance is generally high. Model performance at the Far Site decreases as higher uptake rates (0.24 and 0.36 1/d) are used, due to over-estimation of biotic uptake. In sum, the optimal model has a grid size of 4.5 m near the Farmland Release, a turbulent Schmidt number equal to 1.00, and a nitrate uptake rate of 0.12 1/d.

5. Discussion

We developed a 2-D hydrodynamic model that was fine-tuned using high-frequency nitrate sensor data to better comprehend, with high temporal accuracy, the transport and cycling of nitrate released from a fertilizer plant into a large river. Specifically, we asked: (1) What advantages does integrating high-frequency sensor data offer in understanding biogeochemical processes and improving model evaluation? (2) Can the model accurately predict the magnitude of diel nitrate variations in nitrate dynamics that occur due to biotic assimilation? (3) How sensitive are the model results to variations in grid size, turbulent dispersion, and decay rate, and how does this sensitivity change over space and time?

To the first question, integrating high-frequency sensor data not only "fills the gaps" between discrete grab-samples in a timeseries, providing more model evaluation data, but it also reveals pertinent biochemical processes, such as diel nitrate variability, which are typically not available from sampling at coarser resolutions. This additional layer of knowledge about the system provides us an opportunity to improve our models to have greater fidelity to the processes we seek to simulate. To the second question, we show that while the hydrodynamic model used in this study (MIKE 21) can satisfactorily simulate overall trends observed in the nitrate sensor data, it underestimates the magnitude of diel nitrate variation. This potentially occurs because the reactive module within MIKE 21 is built on first-order kinetics, which some systems may not always exhibit – such as the Kansas River during this prolonged period of unusually high nitrate loading. Lastly, to the third question, we find that turbulent mixing and dispersion dominate nitrate dynamics near the controlled release, but that after a longitudinal distance of approximately 20 river widths, nitrate reactivity becomes a more prominent control.

5.1. Transport of nitrate in a large river system, fine-tuning of dispersion and uptake

Our understanding of the fate of point-source nitrate pollution within downstream water bodies is limited by our ability to accurately predict dispersion (a physical aspect) and uptake (a biochemical aspect), which are influenced by hydrological, biological, and morphological factors (Jung et al., 2019; Kim et al., 2011). While large rivers are known to have considerable mixing due to turbulent flow and complex channel morphology, predicted dispersion coefficients in such rivers vary by an order of magnitude, highlighting the need to improve our understanding of mixing processes (Gond et al., 2021; Pilechi et al., 2016). While it has long been recognized that small streams have a higher nitrate removal efficiency (Peterson et al., 2001), recent studies have also shown that large rivers can play a significant role in retaining and transforming nutrients, thereby reducing their downstream transport (Kelly et al., 2021; Newcomer Johnson et al., 2016). However, the detailed mechanisms that govern these transformations in large rivers are largely unclear. For example, in a study conducted in the same reach as ours, Kelly et al. (2021) did not observe any impact of nutrient saturation in the vicinity of the Farmland Release, which contrasts with previous findings that indicate that high nitrate concentrations can lead to uptake saturation (Wollheim et al., 2018).

Regarding the physical aspects, our best model performance was achieved with a turbulent Schmidt number (S_t) of 1, which falls within the range of turbulent Schmidt numbers reported in the literature (Gualtieri et al., 2017; Tominaga and Stathopoulos, 2007). However, it is important to acknowledge that the value of the turbulent Schmidt number can vary significantly depending on factors such as flow conditions, geometry, and the specific substance being transported. Therefore, direct comparison of our obtained value with other values in the literature can be challenging due to these contextual differences. We purposefully calibrated the turbulent Schmidt number using the Near Site sensor data because the large gradients in longitudinal and lateral concentrations, and the relevance of physical processes as indicated by the Damköhler number. Previous studies have shown mixing coefficients are generally larger at the apex of channel bends (where the Near Site is located) where secondary flows can accelerate the mixing process (Jung et al., 2019). Our findings indicate that the mixing coefficient near the point of release has a significant impact on the accuracy of the model results. For reliable predictions of areas near the release point, it is crucial to calibrate the model using observed data collected from a site located nearby. Otherwise, the model results may not be accurate for those areas. In our case, the nitrate results become independent from the selection of the horizontal dispersion coefficient once the fully mixed condition is reached, which occurred after approximately 20 river widths in the optimal model scenario.

Regarding the biochemical aspects, a nitrogen mass balance of the Kansas River system during the two-month study period showed that 154 tN (metric tons of N) flowed into our study reach from the upstream basin. The controlled release of fertilizer added an additional 60 tN to the study reach, bringing the total N inputs to 214 tN. Assuming conservative conditions in the river, i.e., no biochemical transformation during transport, this would be the amount of nitrogen exported downstream. However, due to modeled nitrogen uptake, which we assume to be entirely biotic assimilation as denitrification rates were measured to be minor (Kelly et al., 2021), this number was lowered from 214 to 185 tN. In sum, uptake of reactive nitrogen accounted for 29 tN of removal, at a rate of 0.10 g-N m^{-2} d^{-1}, which represents 14% of the total river load during this period. Thus, nearly half the fertilizer addition was assimilated within the 33-km reach. This areal uptake rate is comparable to studies of other large, polluted river systems (Finkler et al., 2023; Newcomer Johnson et al., 2016; Rode et al., 2016a). Thus, the Kansas River has some ability to mitigate nitrogen pollution through temporary nitrogen removal.

By utilizing a formulation of uptake rate that takes into consideration the time of day and temperature (Equation 6), diel variations due to biological activity were represented in our model. At the Near Site, while we observed diel patterns in the sensor data (Fig. 3), we observed no noticeable difference in our model performance at the Near Site when applying $\bar{k}_p$ within the range of 0 to 0.36 1/d (Table 2). We largely attribute this insensitivity to the significant nitrogen loading from nearby Farmland Release overriding the modeled nitrate signal. In contrast, our model results for the Far Site, 33-km downstream of the release, were much more sensitive to the uptake parameter. The best model performance was obtained with a mean decay rate of 0.12 1/d (normalized to area: 0.10 g-N m^{-2} d^{-1}), which is smaller than the uptake rate calculated from time-series analysis by Kelly et al. (2021) for the same site (0.58 $\pm$ 0.38 g-N m^{-2} d^{-1}). Model results using larger uptake values (up to 0.36 1/d, corresponding to 0.30 g-N m^{-2} d^{-1}) were within the standard deviation of the Kelly et. al (2021) time-series results but were sub-optimal in terms of overall performance. Differences in uptake estimates between the two methods could be a result of spatial scale: the time-series analysis captures the heterogeneity of a single location using sensor measurements whereas the numerical model simulates the entire reach, introducing homogeneity as fine features are smoothed out. Our calibrated uptake rate was found to be in the range of polluted rivers and streams (Burns et al., 2019; Jarvie et al., 2018) but significantly larger than natural streams (Heffernan and Cohen, 2010; Rode et al., 2016a), suggesting that point-source pollution can influence biogeochemical processes that extend up to tens of kilometers from the release point.

5.2. Integration of high-frequency sensing data into numerical model evaluation

The increasing availability of high-frequency nitrate data provides an opportunity to improve monitoring resolution to the timescales of biogeochemical processes in rivers, which has resulted in a growing

demand to incorporate such data into numerical models (Husic et al., 2023). It is the typical notion that models lose effectiveness when transitioning from coarser to finer time scales, such as from monthly to daily to hourly (Yuan et al., 2020). This is in part due to the fact that the temporal resolution of our historical data observations (sporadically collected at daily-to-monthly periods) did not match the temporal resolution of our model evaluation (continuously simulated at minute-to-hourly scales). In contrast, a major benefit of incorporating high-frequency nitrate data into advection-dispersion-reaction modeling is that the disagreement between temporal frequency of data and models can be closed, i.e., there is a coherence between our observations and simulations. Integrating high-frequency sensor data "fills the gaps" between sporadic grab-samples in a timeseries, providing more model evaluation data to increase confidence in model outputs. Further, high-frequency data discerns intricate details regarding diel variations and rapid fluctuations in nitrate concentration, such as those found near the Farmland Release (Fig. 3), which otherwise might be overlooked with infrequent grab sampling. Thus, richer insights from high-frequency data raise expectations of model fidelity to the "real world" and also expose areas in which our existing models falter.

One way in which high-frequency aquatic sensor data can improve model fidelity is through the identification of sub-daily processes, such as nitrate diel patterns (Fig. 5). Since the proliferation of nitrate sensors in the late 2000's, diel variations have been the subject of study using high-frequency measurements (Burns et al., 2016; Heffernan and Cohen, 2010), but have only recently been integrated numerical model evaluation (Yang et al., 2023). In Burns et al. (2016), estimated C_{diel}/C_{mean} variations in the Potomac River, Maryland, were equal to 0.04 and were attributed to a combination of uptake and denitrification. Heffernan and Cohen (2010) showed greater C_{diel}/C_{max} equal to 0.11 at the spring-fed Ichetucknee River, Florida, which they similarly attributed to both denitrification and uptake. While our modeling results in the Kansas River are in line with reported values (modeled C_{diel}/C_{max} ranged from 0.04 to 0.11), the sensor observations showed much higher C_{diel}/C_{max} values of 0.11 to 0.25. The magnitude of C_{diel}/C_{max} does not necessarily seem tied to nitrate concentration, as the Potomac River ($\overline{C} = 1.09$ mg-N/L) had the largest mean nitrate concentrations compared to the Ichetucknee ($\overline{C} = 0.43$ mg-N/L) and Kansas ($\overline{C} = 0.64$ mg-N/L) Rivers, but the smallest C_{diel}/C_{max}. Differences between our observed diel variations (> 0.11) and those that we modeled and saw reported in the literature (< 0.11) could be due to the unique nutrient loading scenario during this period in the Kansas River. Kelly and others (2021) hypothesized that the microbiome of the Farmland fertilizer ponds was tuned to very high nitrate conditions ($\overline{C} \approx 500$ mg N L^{-1}), thus when discharged into the Kansas River, the biota maintain a high capacity for nutrient removal in their new environment. Lastly, while whole-river denitrification rates in the Kansas River have previously been reported to be low (< 0.02 g-N m^{-2} d^{-1}; Kelly et al., 2021), there could be temporal or spatial heterogeneity of hot spots of denitrification, which could account for some of the nitrate loss beyond what we predicted by assimilatory uptake alone.

High-frequency observations are also useful for determining where our modeling assumptions may falter. The numerical model we use (MIKE 21), like many other models of transport in rivers, assumes that nitrate fate follows a first-order decay, i.e., decay rate is linearly dependent on concentrations. However, the sensor data showed that even with a nearly 50% decrease in mean concentration from February to March (0.82 vs 0.46 mg-N/L), the value of C_{diel} was relatively unchanged (0.10 vs 0.11 mg-N/L), suggesting zero-order behavior, i.e., reactivity is independent of concentration. We looked at ten years of consecutive sensor data in the Kansas River (2013 to 2023), excluding the 2018 year of release, and found similar patterns: similar C_{diel} values in February (0.09 ± 0.06 mg-N/L) and March (0.11 ± 0.14 mg-N/L) despite different nitrate concentrations in February (1.02 ± 0.41 mg-N/L) versus March (0.70 ± 0.50 mg-N/L). This finding suggests that point-source pollution was not the underlying reason for the zero-order behavior. This behavior could be explained by the lower water temperature, less stable hydrology during February, and reduced primary production, which may have led to less biotic activity and thus less nitrate uptake, despite the abundance of nitrate during February (Kelly et al., 2021). Previous studies have also attributed the independence of nitrate uptake on concentrations to the limitation of nitrate uptake by the availability of other nutrients and organic matter (Johnson et al., 2012).

Alternate explanations – other than the breakdown of first-order kinetics – that could be responsible for the divergence of observed diel patterns from the patterns hypothesized by phototrophic activity include (1) heterotrophic activity or release of nitrogen (Yang et al., 2023) and (2) hydraulic transport, dispersion, and storage (Hensley and Cohen, 2016). Yang and others (2013) identify four types of diel uptake patterns from a clustering analysis of 178 days of diel variation in the Lower Bode River, Germany. Our Near Site most closely follows what the authors call a "C1" pattern, which are typical of autotrophic-induced diel variations (crest in the early morning and trough in the late afternoon; Fig. 3). On the other hand, the Far Site showed the opposite behavior, which the authors call a "C4" pattern (trough in the early morning and crest in the afternoon; Fig. 3). This latter pattern is less-explored, but could be the result of redox controls and heterotrophic-related removal, such as denitrification (Zhang et al., 2023), although in our study area measured denitrification rates were low compared to uptake (Kelly et al., 2021). Nitrification is a possibility for the increases in daytime NO_3^- because NH_4^+–N in the fertilizer effluent was highly concentrated (up to 125 mg L^{-1}). However, most samples of NH_4^+ downstream of the release were below the detection limit (Kelly et al., 2021), thus we don't consider this mechanism as the most likely. On the other hand, a non-biochemical reason for the varying diel behavior at the two sites could be the result of physical transport. Storage and transport of upstream nitrogen can cause obscuring of the local biochemical dynamics at a site (Hensley and Cohen, 2016). In our case, we have a large fertilizer release, where upstream diel swings are an order of magnitude greater (for February, C_{diel} was 1.02 ± 0.41 mg-N/L at Near Site and 0.09 ± 0.06 mg-N/L at Far Site), which is then advected downstream at an average of 0.61 m/s. The distance between the sites is approximately 31 km. Thus, the average travel time ($\tau = L/\overline{u}$) is 14 hours, which is not far from the observed time shift (t_{shift} is 8 to 12 hours) between peak NO_3^- at Near Site and Far Site (Fig. 3). Thus, physical transport from the Near Site could account for some of the behavior at the Far Site. However, the fertilizer addition only amounts to 1/4 of the nitrogen in the study reach (3/4 of the nitrogen enters the reach via the Kansas River at the upstream boundary). Further, we observe the same disconnect in first-order behavior at the Far Site even in years without fertilizer additions, thus there must be additional mechanisms at play. While our results point to potential zero-order behavior, more study is required to refine estimates of nitrogen cycling within the Kansas River.

Beyond the processes that may be occurring in the field, there are also limitations regarding how we represent them in models. Numerical models must inherently make some simplifications of the real-world. The model we use, whilst robust and generally performs well, has some structural limitations that pose constraints on fully resolving field measurements. First, MIKE 21 only allows for temporal variation in decay rate and does not account for spatial variability. Allowing for spatial determination of changes in uptake could resolve some discrepancies between sites as redox conditions will vary within a reach (Hubbard et al., 2010; Yang et al., 2019). Second, MIKE 21 considers a single value for bulk nitrate reactivity, which we assume to represent net uptake by all biota within the river system. Other model formulations, such as the Water Quality Analysis Simulation Program (WASP), can differentiate between benthic and pelagic uptake and other reaction pathways (Huang et al., 2022), which has potential for improved model

performance. Third, uncertainties associated with how we defined upstream, lateral, and tributary nitrate and water inputs hindered the model's ability to represent observed conditions. To minimize the assumptions imposed on the model, and because our upstream nitrate sensor malfunctioned, we assumed a constant value for daily nitrate input as the upstream boundary condition (i.e., inputs did not have diel patterns; Figure S2). This forces the model to develop all diel patterns within the study reach, which was only partially accomplished. To improve on this, we would have sensing data to resolve this uncertainty as other authors have done (e.g., Huang et al., 2022; Yang et al., 2023). Despite these areas for improvement, our model is nonetheless robust and performs very well based on comparison to established performance metrics for nitrate models (Wellen et al., 2015).

6. Conclusion

In this study, we sensed and modeled the dispersal and uptake of nitrate following a controlled release of fertilizer into a large river system. The integration of nitrate sensing data into numerical models is an underexplored territory, leaving critical questions about the requisite spatial grid size and temporal resolution needed to effectively interpret sensor readings in numerical models. Notably, our findings reveal that the Near Site, positioned within 0.4 km of the release point, emerged as the most susceptible to variations in river grid size and turbulent mixing parameterization. Conversely, at the Far Site, located 31 km from the release, model performance was largely unaffected by selection of grid size and turbulent mixing, but was rather sensitive to selection of uptake rate. The integration of high-frequency sensor data allowed us to resolve diel variability in nitrate signals, which we incorporated into the model to improve model realism. Regarding nitrate cycling, modeled C_{diel}/C_{max} ranged from 0.04 to 0.11 whereas sensor observations showed much higher C_{diel}/C_{max} values of 0.11 to 0.25. Discrepancies between data observations and model simulations are postulated to result from the breakdown of first-order rate kinetics under variable environmental conditions in the field. The heterogeneity that can occur within the environment is difficult to completely resolve, and simple laboratory-derived relationships often fail to transfer to the field. Nonetheless, leveraging dense datasets that reveal temporal structure, which may otherwise be omitted by traditional sampling, can allow us to identify where models falter and how they can be improved. Together, our study shows the potential of combining numerical models and high-frequency data for a better understanding of the physical and biogeochemical processes that control nitrate dynamics in aquatic environments. Explaining these complexities has the potential to pave the way for improved environmental management and sustainability practices.

CRediT authorship contribution statement

Amirreza Zarnaghsh: Conceptualization, Methodology, Formal analysis, Software, Visualization, Writing – original draft, Writing – review & editing. **Michelle Kelly:** Investigation, Data curation, Writing – review & editing. **Amy Burgin:** Investigation, Data curation, Writing – review & editing. **Admin Husic:** Conceptualization, Methodology, Formal analysis, Visualization, Supervision, Writing – original draft, Writing – review & editing.

Declaration of competing interest

The authors declare that they have no known competing financial interests or personal relationships that could have appeared to influence the work reported in this paper.

Data availability

The data used has been attached as an Excel file.

Acknowledgements

We thank the Department of Civil, Environmental, and Architectural Engineering at the University of Kansas for providing partial support to the lead student-author of this manuscript. We are deeply appreciative of the Danish Hydraulic Institute for providing a student license to the MIKE software free of charge. We are grateful for funding by an NSF DEB-Ecosystems RAPID grant (#1822960) to Dr. Lydia Zeglin and Dr. Amy Burgin, which resulted in the data collection that made this numerical modeling study possible. Further, we thank researchers and stakeholders who supported the field work, data collection, and sensor maintenance, including: Maddy Foster, James Guinnip, Janaye Hanschu, Brandon Kannady, Terry Loecke, Priscilla Moley, Richard Nguyen, Emma Overstreet, Abagael Pruitt, Anne Schechner, Cay Thompson, Dr. Walter Dodds, Dr. Steve Thomas, Dawn and Dennis Buehler, the Friends of the Kaw, the Bowersock Mills and Power Company, the City of Lawrence Municipal Services & Operations Department, the USGS Kansas Water Science Center, and local landowners. Lastly, we thank three anonymous reviewers for their constructive suggestions, which helped improve the quality of this manuscript. We declare no conflicts of interests.

Supplementary materials

Supplementary material associated with this article can be found, in the online version, at doi:10.1016/j.advwatres.2024.104693.

References

AIMS, 2020. Johnson County Automated information Mapping System [WWW Document]. URL https://aims.jocogov.org/(accessed 1.7.20).
Baek, K.O., Seo, I.W., 2016. On the methods for determining the transverse dispersion coefficient in river mixing. Adv. Water Resour. 90, 1–9. https://doi.org/10.1016/j.advwatres.2016.01.009.
Burns, D.A., Miller, M.P., Pellerin, B.A., Capel, P.D., 2016. Patterns of diel variation in nitrate concentrations in the Potomac River. Freshw. Sci. 35, 1117–1132. https://doi.org/10.1086/688777.
Burns, D.A., Pellerin, B.A., Miller, M.P., Capel, P.D., Tesoriero, A.J., Duncan, J.M., 2019. Monitoring the riverine pulse: Applying high-frequency nitrate data to advance integrative understanding of biogeochemical and hydrological processes. Wiley Interdiscip. Rev. Water e1348. https://doi.org/10.1002/wat2.1348.
Camacho Suarez, V.V., Schellart, A.N.A., Brevis, W., Shucksmith, J.D., 2019. Quantifying the Impact of Uncertainty within the Longitudinal Dispersion Coefficient on Concentration Dynamics and Regulatory Compliance in Rivers. Water Resour. Res. 55, 4393–4409. https://doi.org/10.1029/2018WR023417.
Danish Hydraulic Institute, 2019. Hydrodynamic Module User Guide. MIKE 21 Flow Model, Denmark.
Dupas, R., Jomaa, S., Musolff, A., Borchardt, D., Rode, M., 2016. Disentangling the influence of hydroclimatic patterns and agricultural management on river nitrate dynamics from sub-hourly to decadal time scales. Sci. Total Environ. 571, 791–800. https://doi.org/10.1016/j.scitotenv.2016.07.053.
Finkler, N.R., Gücker, B., Cunha, D.G.F., 2023. Nutrient uptake in tropical rivers receiving wastewater treatment plant discharge: High mass removal but low nutrient uptake efficiencies. Ecol. Indic. 154 https://doi.org/10.1016/j.ecolind.2023.110865.
Gond, L., Mignot, E., Le Coz, J., Kateb, L., 2021. Transverse Mixing in Rivers With Longitudinally Varied Morphology. Water Resour. Res. 57, 1–19. https://doi.org/10.1029/2020WR029478.
Gualtieri, C., Angeloudis, A., Bombardelli, F., Jha, S., Stoesser, T., 2017. On the values for the turbulent schmidt number in environmental flows. Fluids 2. https://doi.org/10.3390/fluids2020017.
Gupta, H.V., Kling, H., Yilmaz, K.K., Martinez, G.F., 2009. Decomposition of the mean squared error and NSE performance criteria: Implications for improving hydrological modelling. J. Hydrol. 377, 80–91. https://doi.org/10.1016/j.jhydrol.2009.08.003.
Hansen, A., Singh, A., 2018. High-Frequency Sensor Data Reveal Across-Scale Nitrate Dynamics in Response to Hydrology and Biogeochemistry in Intensively Managed Agricultural Basins. J. Geophys. Res. Biogeosciences 123, 1–15. https://doi.org/10.1029/2017JG004310.
Heffernan, J.B., Cohen, M.J., 2010. Direct and indirect coupling of primary production and diel nitrate dynamics in a subtropical spring-fed river. Limnol. Oceanogr. 55, 677–688. https://doi.org/10.4319/lo.2009.55.2.0677.
Hensley, R.T., Cohen, M.J., 2016. On the emergence of diel solute signals in flowing waters. Water Resour. Res. 52, 759–772. https://doi.org/10.1002/2015WR017895.
Huang, J., Borchardt, D., Rode, M., 2022. How do inorganic nitrogen processing pathways change quantitatively at daily, seasonal, and multiannual scales in a large agricultural stream? Hydrol. Earth Syst. Sci. 26, 5817–5833. https://doi.org/10.5194/hess-26-5817-2022.

Hubbard, K.A., Lautz, L.K., Mitchell, M.J., Mayer, B., Hotchkiss, E.R., 2010. Evaluating nitrate uptake in a Rocky Mountain stream using labelled 15N and ambient nitrate chemistry. Hydrol. Process. 24, 3322–3336. https://doi.org/10.1002/hyp.7764.

Husic, A., Fox, J.F., Clare, E., Mahoney, T., Zarnaghsh, A., 2023. Nitrate hysteresis as a tool for revealing storm-event dynamics and improving water quality model performance. Water Resour. Res. 59, e2022WR033180 https://doi.org/10.1029/2022WR033180.

Jan, A., Coon, E.T., Painter, S.L., 2021. Toward more mechanistic representations of biogeochemical processes in river networks: Implementation and demonstration of a multiscale model. Environ. Model. Softw. 145, 105166 https://doi.org/10.1016/j.envsoft.2021.105166.

Jarvie, H.P., Sharpley, A.N., Kresse, T., Hays, P.D., Williams, R.J., King, S.M., Berry, L., 2018. Coupling high-frequency stream metabolism and nutrient monitoring to explore biogeochemical controls on downstream nitrate delivery. Environ. Sci. Technol. https://doi.org/10.1021/acs.est.8b03074.

Jeon, T.M., Baek, K.O., Seo, I.W., 2007. Development of an empirical equation for the transverse dispersion coefficient in natural streams. Environ. Fluid Mech. 7, 317–329. https://doi.org/10.1007/s10652-007-9027-6.

Johnson, L.T., Royer, T.V., Edgerton, J.M., Leff, L.G., 2012. Manipulation of the Dissolved Organic Carbon Pool in an Agricultural Stream: Responses in Microbial Community Structure, Denitrification, and Assimilatory Nitrogen Uptake. Ecosystems 15, 1027–1038. https://doi.org/10.1007/s10021-012-9563-x.

Jung, S.H., Seo, I.W., Kim, Y.Do, Park, I., 2019. Feasibility of Velocity-Based Method for Transverse Mixing Coefficients in River Mixing Analysis. J. Hydraul. Eng. 145, 1–15. https://doi.org/10.1061/(asce)hy.1943-7900.0001638.

Kelly, M.C., Zeglin, L.H., Husic, A., Burgin, A.J., 2021. High Supply, High Demand: A Fertilizer Waste Release Impacts Nitrate Uptake and Metabolism in a Large River. J. Geophys. Res. Biogeosciences 126. https://doi.org/10.1029/2021JG006469 e2021JG006469.

Kim, K.C., Park, G.H., Jung, S.H., Lee, J.L., Suh, K.S., 2011. Analysis on the characteristics of a pollutant dispersion in river environment. Ann. Nucl. Energy 38, 232–237. https://doi.org/10.1016/j.anucene.2010.11.003.

Knapp, J.L.A., González-Pinzón, R., Drummond, J.D., Larsen, L.G., Cirpka, O.A., Harvey, J.W., 2017. Tracer-based characterization of hyporheic exchange and benthic biolayers in streams. Water Resour. Res. 53, 1575–1594. https://doi.org/10.1002/2016WR019393.

Kunz, J.V., Helsey, R., Brase, L., Borchardt, D., Rode, M., 2017. High frequency measurements of reach scale nitrogen uptake in a fourth order river with contrasting hydromorphology and variable water chemistry (Weiße Elster, Germany). Water Resour. Res. 53, 328–343. https://doi.org/10.1002/2015WR017464.

Ledford, S.H., Toran, L., 2020. Downstream evolution of wastewater treatment plant nutrient signals using high-temporal monitoring. Hydrol. Process. 34, 852–864. https://doi.org/10.1002/hyp.13640.

Lee, M.E., Seo, I.W., 2010. 2D finite element pollutant transport model for accidental mass release in rivers. KSCE J. Civ. Eng. 14, 77–86. https://doi.org/10.1007/s12205-010-0077-9.

Lloyd, C.E., Freer, J.E., Johnes, P.J., Collins, A.L., 2016. Using hysteresis analysis of high-resolution water quality monitoring data, including uncertainty, to infer controls on nutrient and sediment transfer in catchments. Sci. Total Environ. 543, 388–404. https://doi.org/10.1016/j.scitotenv.2015.11.028.

Newcomer Johnson, T.A., Kaushal, S.S., Mayer, P.M., Smith, R.M., Sivirichi, G.M., 2016. Nutrient retention in restored streams and rivers: A global review and synthesis. Water (Switzerland) 8, 1–28. https://doi.org/10.3390/w8040116.

Ocampo, C.J., Oldham, C.E., Sivapalan, M., 2006. Nitrate attenuation in agricultural catchments: Shifting balances between transport and reaction. Water Resour. Res. 42, 1–16. https://doi.org/10.1029/2004WR003773.

Peterson, B.J., Wollheim, W.M., Mulholland, P.J., Webster, J.R., Meyer, J.L., Tank, J.L., Marti, E., Bowden, W.B., Vallett, H.M., Hershey, A.E., McDowell, W.H., Dodds, W.K., Hamilton, S.K., Gregory, S., Morrall, D.D., 2001. Control of nitrogen export from headwaters by headwater streams. Science (80-.) 292, 86–90. https://doi.org/10.1126/science.1056874.

Pilechi, A., Mohammadian, A., Rennie, C.D., Zhu, D.Z., 2016. Efficient Method for Coupling Field Data and Numerical Modeling for the Estimation of Transverse Mixing Coefficients in Meandering Rivers. J. Hydraul. Eng. 142, 04016009 https://doi.org/10.1061/(asce)hy.1943-7900.0001116.

Ramezani, M., Noori, R., Hooshyaripor, F., Deng, Z., Sarang, A., 2019. Numerical modelling-based comparison of longitudinal dispersion coefficient formulas for solute transport in rivers. Hydrol. Sci. J. 64, 808–819. https://doi.org/10.1080/02626667.2019.1605240.

Reay, D.S., Nedwell, D.B., Priddle, J., Ellis-Evans, J.C., 1999. Temperature dependence of inorganic nitrogen uptake: Reduced affinity for nitrate at suboptimal temperatures in both algae and bacteria. Appl. Environ. Microbiol. 65, 2577–2584. https://doi.org/10.1128/aem.65.6.2577-2584.1999.

Rode, M., Halbedel Née Angelstein, S., Anis, M.R., Borchardt, D., Weitere, M., 2016a. Continuous In-Stream Assimilatory Nitrate Uptake from High-Frequency Sensor Measurements. Environ. Sci. Technol. 50, 5685–5694. https://doi.org/10.1021/acs.est.6b00943.

Rode, M., Wade, A.J., Cohen, M.J., Hensley, R.T., Bowes, M.J., Kirchner, J.W., Arhonditsis, G.B., Jordan, P., Kronvang, B., Halliday, S.J., Skeffington, R.A., Rozemeijer, J.C., Aubert, A.H., Rinke, K., Jomaa, S., 2016b. Sensors in the Stream: The High-Frequency Wave of the Present. Environ. Sci. Technol. 50, 10297–10307. https://doi.org/10.1021/acs.est.6b02155.

Rodi, W., 2000. Turbulence models and their application in hydraulics : a state-of-the art review, 3rd ed. International Association for Hydro-Environment Engineering and ResearchCRC Press, Rotterdam, Netherlands.

Shen, H., Tolson, B.A., Mai, J., 2022. Time to Update the Split-Sample Approach in Hydrological Model Calibration. Water Resour. Res. 58, 1–26. https://doi.org/10.1029/2021WR031523.

Shin, J., Seo, I.W., Baek, D., 2020. Longitudinal and transverse dispersion coefficients of 2D contaminant transport model for mixing analysis in open channels. J. Hydrol. 583, 124302 https://doi.org/10.1016/j.jhydrol.2019.124302.

Tominaga, Y., Stathopoulos, T., 2007. Turbulent Schmidt numbers for CFD analysis with various types of flowfield. Atmos. Environ. 41, 8091–8099. https://doi.org/10.1016/j.atmosenv.2007.06.054.

van Genuchten, M.T., Leij, F.J., Skaggs, T.H., Toride, N., Bradford, S.A., Pontedeiro, E.M., 2013. Exact analytical solutions for contaminant transport in rivers 1. The equilibrium advection-dispersion equation. J. Hydrol. Hydromechanics 61, 146–160. https://doi.org/10.2478/johh-2013-0020.

Velísková, Y., Sokáč, M., Halaj, P., Koczka Bara, M., Dulovičová, R., Schügerl, R., 2014. Pollutant Spreading in a Small Stream: A Case Study in Mala Nitra Canal in Slovakia. Environ. Process. 1, 265–276. https://doi.org/10.1007/s40710-014-0021-y.

Wellen, C., Kamran-Disfani, A.-R., Arhonditsis, G.B., 2015. Evaluation of the Current State of Distributed Watershed Nutrient Water Quality Modeling. Environ. Sci. Technol. 49, 3278–3290. https://doi.org/10.1021/es5049557.

Wollheim, W.M., Bernal, S., Burns, D.A., Czuba, J.A., Driscoll, C.T., Hansen, A.T., Hensley, R.T., Hosen, J.D., Inamdar, S., Kaushal, S.S., Koenig, L.E., Lu, Y.H., Marzadri, A., Raymond, P.A., Scott, D., Stewart, R.J., Vidon, P.G., Wohl, E., 2018. River network saturation concept: factors influencing the balance of biogeochemical supply and demand of river networks. Biogeochemistry 141, 503–521. https://doi.org/10.1007/s10533-018-0488-0.

Yang, X., Jomaa, S., Büttner, O., Rode, M., 2019. Autotrophic nitrate uptake in river networks: A modeling approach using continuous high-frequency data. Water Res 157, 258–268. https://doi.org/10.1016/j.watres.2019.02.059.

Yang, X., Zhang, X., Graeber, D., Hensley, R., Jarvie, H., Lorke, A., Borchardt, D., Li, Q., Rode, M., 2023. Large-stream nitrate retention patterns shift during droughts: Seasonal to sub-daily insights from high-frequency data-model fusion. Water Res 243, 120347. https://doi.org/10.1016/j.watres.2023.120347.

Yuan, L., Sinshaw, T., Forshay, K.J., 2020. Review of watershed-scale water quality and nonpoint source pollution models. Geosci 10, 1–33. https://doi.org/10.3390/geosciences10010025.

Zarnaghsh, A., Husic, A., 2023. An index for inferring dominant transport pathways of solutes and sediment: Assessing land use impacts with high-frequency conductivity and turbidity sensor data. Sci. Total Environ., 164931 https://doi.org/10.1016/j.scitotenv.2023.164931.

Zhang, X., Yang, X., Hensley, R., Lorke, A., Rode, M., 2023. Disentangling In-Stream Nitrate Uptake Pathways Based on Two-Station High-Frequency Monitoring in High-Order Streams. Water Resour. Res. 59, 1–17. https://doi.org/10.1029/2022WR032329.